Laser diagnostic design for the EPAC EA1 beamline

Contact: thomas.dzelzainis@stfc.ac.uk

T. Dzelzainis, A. Stallwood, & D. R. Symes
Central Laser Facility, Rutherford Appleton Laboratory, Didcot OX11 0QX, United Kingdom

Introduction

EPAC Experimental Area 1 will house a long-focus PW laser beamline primarily designed for laser-wakefield acceleration in gas targets. This has been described in the previous CLF annual report [1]. In this report, we describe in more detail the diagnostics that will be used to characterise and monitor the laser beam. The first diagnostic measures the properties of the beam entering EA1 by taking a leakage through the final turning mirror in the beamline – this will be used for daily alignment and on-shot beam monitoring. The second diagnostic characterises the laser pulse after it has passed through the plasma – modifications to the spectral and spatial profile of the beam provide important information for understanding the physics of the LWFA interaction.

The layout of the input beam diagnostic is shown in Fig. 1. The diagnostic has been designed using Zemax software for the full size (220 mm diameter) main beam at 800 nm wavelength (IR), and a pilot beam (injected for the stabilisation system) with diameter up to 220 mm and wavelength 405 nm (blue). An internal EA1 beam – designed as a 100 mm diameter CW beam at 532 nm for preliminary experimental alignment – will be partially reflected onto both sets of diagnostics. The diagnostic beam is derived from the leakage through the final turning mirror that steers the beam into the EA1 beamline. It exits the vacuum system through a plane-parallel window tilted at a small angle to avoid direct back reflections into the laser. This window will have a partially reflective coating applied to reduce B-integral in the diagnostic line. The beam is reflected from a silver-coated mirror [M1] and passes through an uncoated, wedged optic [M3] before being focused by the primary focussing optic – a 6600 mm focal length (f / 30) silver-coated spherical mirror [M2] – used at normal incidence. The reflection from the spherical mirror is isolated by taking the reflection of the focussing beam from M3 on its return pass. The wedge ensures that the unwanted rear surface reflection can be identified and eliminated. The wedged optic is used with a small angle of incidence to minimise aberrations. After reflection from M3, the focussing beam is folded by a 6" diameter silver-coated mirror [M4] and directed to a periscope [M5/M6] that drops the beam to a more convenient height for the small optics used with the condensed beam. The optics here are also used to provide filtering for full power shots. To accomplish this, two periscopes are mounted on a translation stage so that either periscope can be used in the beamline. One periscope, used for alignment, will have highly reflective (HR) silver-coated mirrors, and the second – used for full power shots – will have dielectric coatings that are anti-reflective (AR) at 800 nm, providing a factor of $\sim 10^5$ (assuming 0.5% reflection) attenuation for the main beam. The dielectric coatings can be specified to provide the same throughput for the alignment (532 nm) and stabilisation beams (405 nm) as the first periscope. In this way, the near-field (NF) and far-field (FF) diagnostics can be used to confirm that exchanging periscopes has no effect on the beam pointing, or to correct pointing changes if it does. An alternative scheme could be employed that avoids the need for moving components to improve stability. This would use partial reflectors to split and combine the beam, with the two periscopes (HR and AR) placed in the reflective and transmissive arms with equal path lengths. The diagnostic beam path would be determined using motorised beam blocks depending on the selected power mode. These two options will be considered during installation.

After the periscope, a dielectric optic [M7] transmits most of the 405 nm pilot beam to reach a position sensitive detector (PSD). By minimising the number of reflections prior to focus, and by avoiding reflections from small optics, this position for the PSD maximises stability. (Smaller optics are expected to suffer more thermal drift because of the shorter distance between pivot and actuator, meaning the resulting angular change for a given change in actuator length is larger.) The IR beam, and reflected blue beam are directed to a dichroic mirror [M8] where the remaining blue light is transmitted to NF and FF monitors, and the IR beam is reflected to reach the primary focus. After focus, the IR beam is collimated using a 125 mm focal length lens to produce a beam of diameter 4.2 mm. It is then image relayed through a 1:1 telescope to provide a more convenient image plane After the telescope, the beam is split into separate channels for NF, FF and wavefront diagnostics. The relay telescope is placed after a dog-leg to allow easy alignment, and avoids the introduction of wave-front errors or chromatic aberration by using large f / # (of order f / 70) achromatic doublets optimised near 800 nm. The selected beamsize of 4.2 mm is compatible with the sensor size for AVT Manta cameras, and is also suitable for use with the HASO-4 we expect to use. The FF is shown

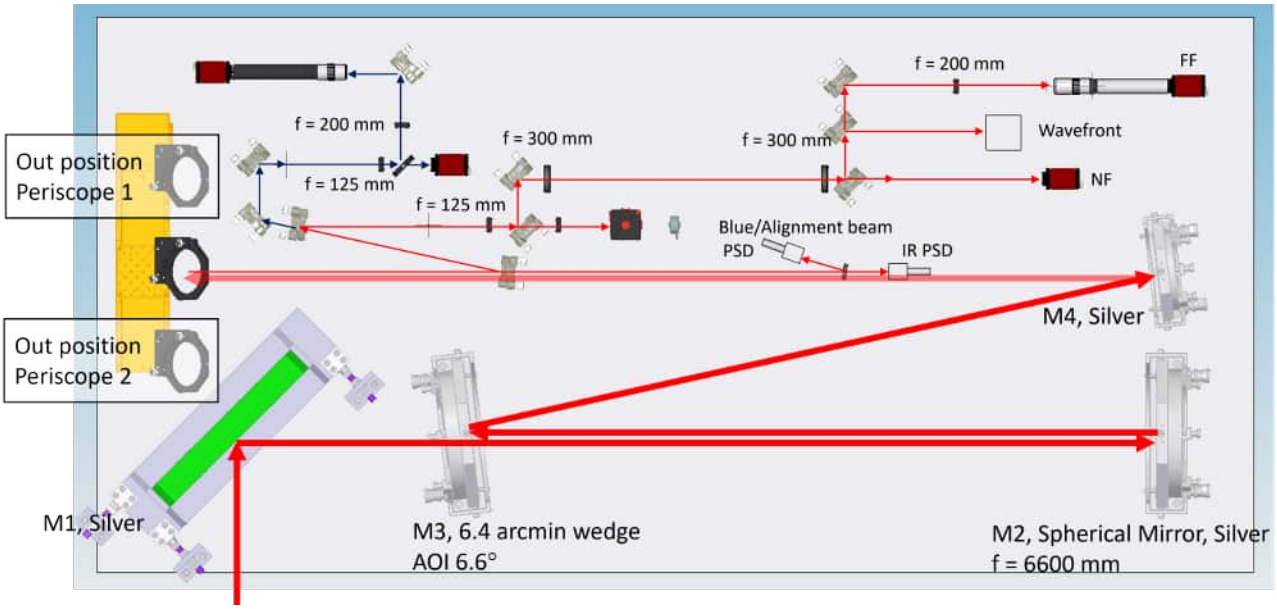

Figure 1: Proposed design for the diagnostic layout used for monitoring the beam entering the EA1 beamline

using an f / 60 achromatic doublet – this focal length could be reduced if needed without introducing significant aberration. The integrating sphere, which can be used for both a spectral measurement and energy measurement, has no requirement for wavefront quality or imaging, and so is placed on the leakage from the first mirror of the dog-leg. Any simple lens can be used to focus the beam into the integrating sphere head without a relay telescope. If the beam diameter is smaller than the detector area, then no lens is needed. The layout has flexibility to accommodate different beam diameters if required, and there is space for an additional diagnostic to be positioned to use the leakage from the second dog-leg mirror.

The object plane used for the imaging systems has been set to be 50 metres before the leakage mirror. This plane is imaged onto the lens array of the HASO, the sensor location of the NF camera, and the lens focussing the beam onto the FF camera. This ensures that the wavefront, NF, and FF are all sampled at equivalent planes. Because the imaging systems are all telecentric, the object plane can be varied without changing magnification simply by moving the detectors. Figure 2 plots the calculated image distance for the range of object distances up to 100 m. These positions can be finessed during installation to image a suitable plane in the laser system (i.e. a particular optic surface, or an alignment reference). The object plane could also be moved closer – for example to the leakage mirror surface – or to negative position allowing a measurement of the expected NF and wavefront at the AO. There is an upper limit on the imaging distance, as the detector is required to move closer to the telescope output lens, but even an object plane at a distance of >100 m can be imaged.

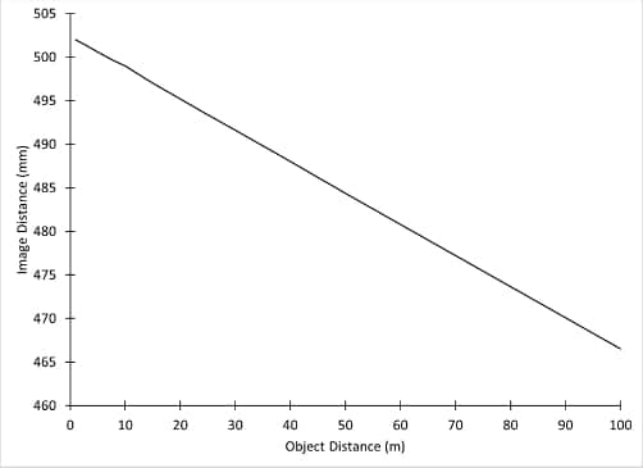

Figure 2: Calculated image distance as a function of object distance up to 100 m.

Design details

A primary requirement of the diagnostic design was to achieve aberration free imaging and focussing of the beam. Ignoring manufacturing errors, the remaining sources of aberration are those inherent to the focussing optic, e.g. spherical aberration, and those that may arise due to misalignment. Any design should attempt to make these sources of aberration negligible when compared to surface tolerances. Therefore it must not just produce a theoretically aberration free system, but also must provide tolerances on alignment, as well as a realistic method to reach those tolerances. As manufacturing tolerances on optical surfaces are typically λ / 10, a target of λ / 100 was set for the wavefront error.

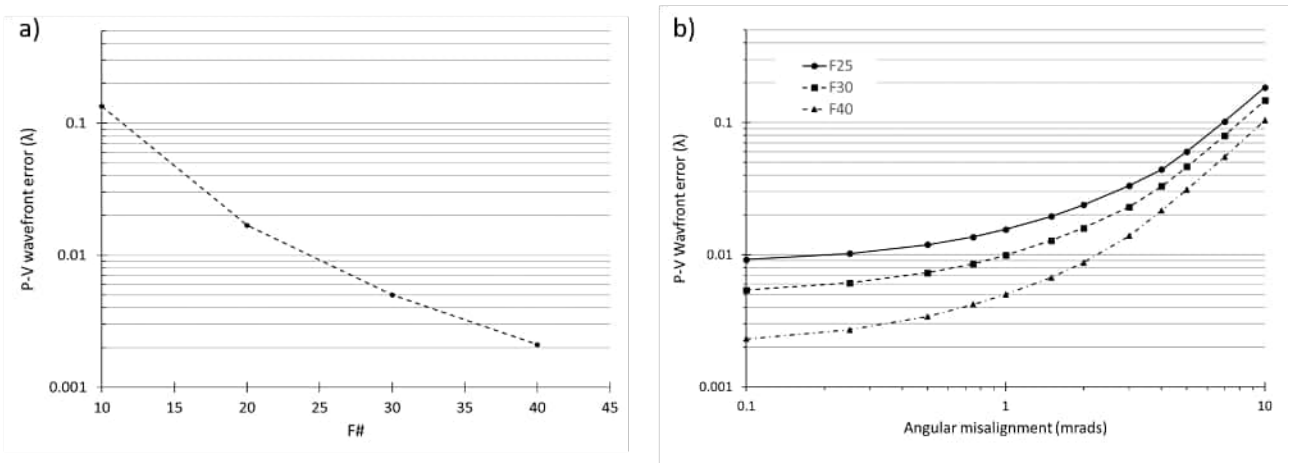

Figure 3: a) Peak-to-valley wavefront error for a spherical mirror as a function of f/#; b) peak-to-valley wavefront error as a function of angular misalignment for f / 25, f / 30 and f / 40 mirrors

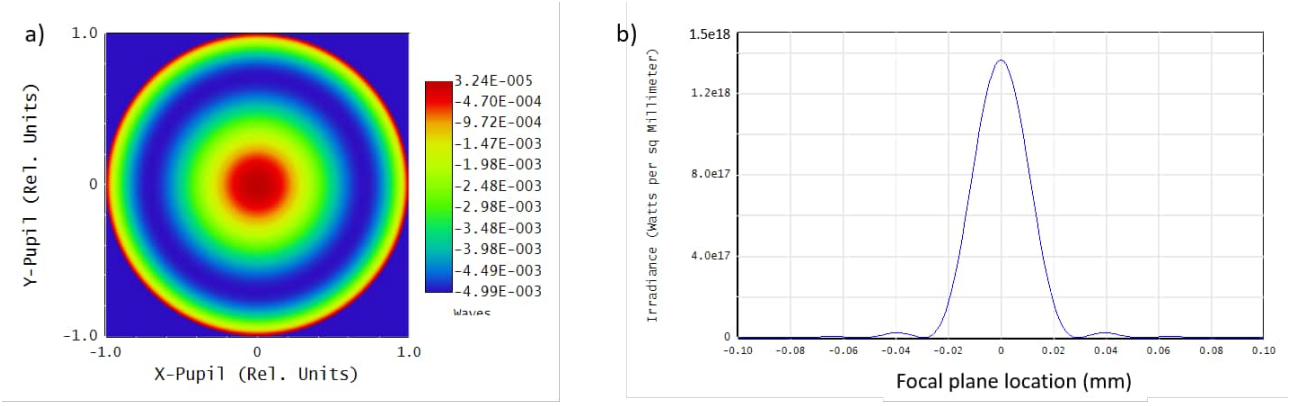

Figure 4: a) Wavefront map of primary focus showing 0.005 waves of aberration; b) line-out of corresponding spot in x-direction at focus

Selection of primary focusing optic

For reasons discussed below, we have chosen a spherical mirror for the focusing optic in this diagnostic. A plot showing peak-to-valley (P-V) wavefront error as a function of f/# for a spherical mirror is shown in Fig. 3 a). It can be seen that the inherent aberration drops below λ / 100 at $\sim$ f / 25, which sets a lower limit on the required focal length to remove this aberration. The simplicity of the alignment method for a spherical mirror means that it is straightforward to estimate the expected aberration due to angular misalignment. Because of its symmetry, a spherical mirror has no defined optical axis and so, as long as the beam remains within the clear aperture, exact centring of the beam on the optic is unnecessary and the only alignment required is direct back reflection of the beam. The expected accuracy depends only on how well the back-reflected beam can be positioned w.r.t. the incoming beam, which in turn depends on a) where the back reflected beam can be observed, and b) how accurately the centre of the expanded beam can be defined. Figure 3 b) shows P-V wavefront error as a function of angular misalignment for f / 25, f / 30, and f / 40 spherical mirrors. It can be seen that the required angular alignment accuracy is quite relaxed. An accuracy of 1 mrad would ensure aberrations are entirely negligible ($< \lambda$ / 100). This corresponds to a requirement that the back-reflected beam is overlapped with the incoming beam to an accuracy of $\pm$ 6 mm at the position of the leakage mirror (approximately 3 m from the spherical mirror surface). This should be achievable, and will be mainly determined by how well the centre of the beam can be defined rather than inaccuracy setting the angle of the spherical mirror.

The calculated wavefront map and a line-out at the plane of the primary focus, is shown in Fig. 4. The intensity in the lineout is given in W mm^{-2}, assuming an input beam intensity of 2.63 x 10^{10} W mm^{-2}. This corresponds to the full energy EPAC pulse (30 J) with 100% throughput for all optics. This value will need to be adjusted to account for the real transmission of the optics in the chain when this information is known.

Alternative focusing options

Alternative options for the primary focusing optic were considered during design: a) lenses, and b) off-axis parabolas (OAPs). In both cases the main advantage over the normal-incidence spherical-mirror option is the lack of a requirement to use a wedge to separate the incoming beam from the focussing beam. The wedge in the system makes alignment more difficult because the beam is significantly weaker after reflection. However, this is a relatively minor inconvenience as the diagnostic can mostly be aligned using overlapped visible beams. The alignment difficulty is out-weighed by the disadvantages identified below for lenses and OAPs.

Lenses suffer two main drawbacks compared to spherical mirrors. Firstly, for the same f/#, a plano-convex spherical lens introduces more aberration than a spherical mirror — Figure 5 a) shows the P-V wavefront error for a spherical lens as a function of f/#. It shows that $>$ f / 50 focussing would be required to reduce spherical aberration to negligible levels. The second disadvantage of a lens is chromatic aberration. Both spherical and aspherical lenses suffer to similar degrees. This can be reduced by further increasing the f/#. Figure 5 b) shows the ratio of the rms spot radius calculated using geometric ray-tracing to the radius of the first Airy minimum. It shows that any singlet lens would have to be roughly f / 60 before it would focus a 30 nm bandwidth without noticeable chromatic aberration. Both spherical and chromatic aberration can be largely eliminated by the use of an appropriately designed achromat. However, even an air-spaced doublet would at least double the cost of the focussing optic compared to a singlet.

OAPs are more expensive than spherical mirrors, but provide achromatic, aberration free performance for any f/#, meaning a shorter focal length could be used. However OAPs are time-consuming and complicated to align and to check, in contrast with the simplicity of aligning a spherical mirror. This leads to uncertainty whether measured aberrations arise in the diagnostic rather than being present in the beam. In addition, while shorter focal lengths reduce the footprint of the diagnostic, the longer focal length arrangement has some benefits: the system is more tolerant to alignment inaccuracies; the focusing beam can be transmitted through subsequent near normal incidence optics without introducing significant aberration; and more space is available for beam manipulation and filtering optics. Finally, the f/# of the initial optic is maintained through the subsequent imaging systems, so a large f/# ensures that the relay telescope optics will not be a later source of aberration.

Correction of angular dispersion

The turning mirror in the beam transport line has a wedged rear surface, meaning that the leakage beam picks up some angular dispersion as it is transmitted. This would increase the focal spot size in the direction of the angular dispersion. The impact on the diagnostic is a distortion of the spot on the FF camera, and a reduction in the accuracy of the measurement of centroid positions in the wavefront monitor. It would also leave the wavefront monitor sensitive to changes in the spectrum, as a change in the spectrum of the laser could result in a shift in measured centroid position. The problem can be avoided by selecting the angle of the diagnostic wedge [M3] to compensate for the angular dispersion introduced through the mirror. The only constraint being that the wedge angle must be large enough to allow the separation of front and back reflections both during alignment and at the individual detectors. The leakage mirror has been specified to have a wedge of 4 arcmins - this allows a reflection from the rear surface to be used as pilot beam for on-target beam pointing stability. In order to remove angular dispersion, the size of the wedge in the diagnostic line was chosen as 6.4 arcmin. The difference in wedge angles is due to the different angle of incidence for the two optics. The angular dispersion can be almost perfectly corrected for wavelengths of interest (800 nm, 532 nm, 405 nm) down to 400 nm, with the only resulting distortion being a lateral displacement of different wavelengths as a result of travelling a finite distance before the angular dispersion is corrected. However this is approximately 20 microns across the 60 nm bandwidth of the main beam, and so can be ignored. The displacement at 400 nm is larger, at $\sim$ 350 micron, but still negligible in terms of NF alignment. As both the NF and FF displacements due to angular dispersion have been reduced to negligible levels, the alignment of the diagnostic system can be carried out using a laser of any wavelength - provided that it is well overlapped with the main beam with references in the beamline.

Separation of front- and rear-surface reflections

The separation of the front and rear reflections from the wedge can be challenging, especially with small wedge angles. Due to the physical separation of the points of reflection the two beams will start off with a lateral shift at the wedge surface and then this separation increases with distance travelled due to their angular separation. For the wedge specified in the design (fused silica, 40 mm thickness, 6.4 arcmins wedge angle, used at 6.6 degree angle of incidence) the front and rear reflections will have a separation of slightly over 6 mm at the wedge surface, increasing to 12 mm at the first fold mirror [M4]. By placing an iris in the beam before transmission through the wedge the correct beam can be identified and aligned. At the primary focus, the front and rear reflections will be separated by approximately 25 mm so it will be straightforward to block the rear surface reflection. This separation also applies to the pilot beam, meaning that the rear-surface reflection will not interfere with the pilot beam PSD signal.

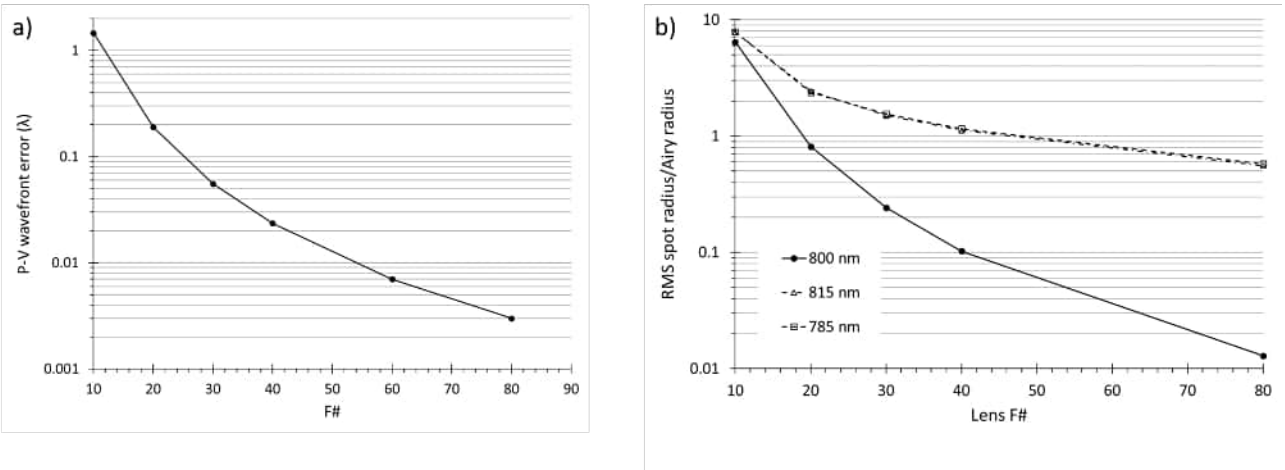

Figure 5: a) P-V wavefront error as a function of f/# for a plano-convex spherical lens; b) ratio of rms spot radius (obtained by geometrical optics), to the radius of the first Airy minimum for wavelengths representative of the EPAC bandwidth, for a plano-convex spherical lens optimised for 800 nm light.

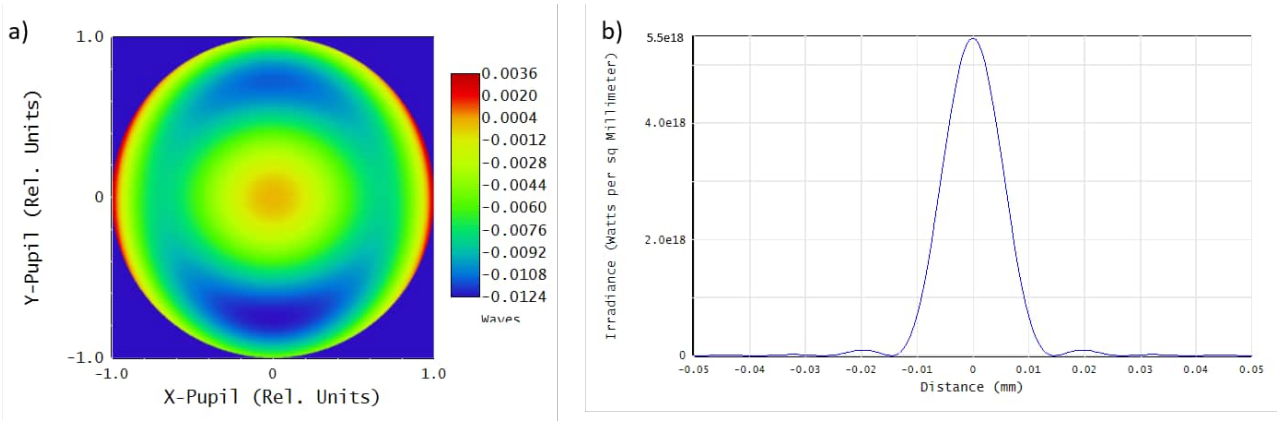

Figure 6: a) Wavefront map and b) line-out through focal spot for PSD focus for 400 nm pilot beam assuming 220mm expanded beam diameter.

Focusing of the pilot beam

The position sensitive detector is placed on the leakage beam of mirror M7, and the blue beam NF/FF lines on the leakage of M8. Being so similar, the channels show near-identical performance. In both cases the focussing beam passes through an optic, causing aberration. However, this aberration is kept negligible by using near normal angle of incidence and a large f/# for the focussing cone. Figure 6 shows (a) the wavefront error in the beam at PSD focus, with a P-V error of ~ 0.016, and (b) corresponding intensity distribution at focus. We can therefore expect a diffraction limited performance in both the pilot beam PSD channel, and the 405 nm NF/FF line.

Focusing of the main beam

In the standard configuration, the spherical mirror will produce an image of the grating surface (assumed to be 50 m upstream) 7,604 mm from the mirror surface (1,004 mm after the primary focus), where the beam would be 33.5 mm diameter. Because the beam is collimated before reaching this image plane (by a lens of 125 mm focal length placed 125 mm after focus) the image is formed 110 mm after the collimation lens and the beam size is 4.2 mm diameter. As the beamline is optimised for transport of the parallel beam, aberrations are introduced when used for imaging a point source. To get the best resolution will involve including an aperture somewhere in the system to exclude marginal rays that fall outside of the diffraction limited diameter. There is an obvious trade off as reducing the aperture reduces aberrations, decreasing the spot footprint from the raytrace, but increases the diffraction limited resolution. Therefore the optimum aperture would be one that gives a spot footprint with an RMS diameter $\sim$0.5 times the Airy disc diameter. A reasonable choice for the aperture position would be after the output lens of the relay telescope. Figure 7 gives some key metrics of the collimated

main beamline: a) displays a wavefront map, showing a P-V error of $\sim$ 0.0058 λ; b) displays a beam footprint, demonstrating that negligible distortion is expected in the image plane; and c) shows the spot obtained from a raytrace of the system using an on-axis point source 50 m before the spherical lens, giving a RMS diameter of approximately 17 μm at the image plane. The system has a demagnification of 33, indicating a resolution limit of $\sim$ 560 μm at the object plane. For this simulation, the beam was apertured down to 9 mm at the collimation lens, however such an aperture would not be needed in the real set-up, as the system stop would be an aperture after the relay telescope.

Image relay telescopes

The image relay telescopes for both the HASO and the IR NF/FF channels consist of two lenses of f = 300 mm, separated by 2f. This maintains a collimated output beam 4.2 mm in diameter, and provides an image plane at a convenient distance from the second telescope lens, which allows the beam to be split into different diagnostic channels. The image plane of the collimation lens is taken as the object plane for the relay telescopes, resulting in a final image $\sim$484 mm from the second telescope lens (compared to the image plane of the initial collimation lens, which is $\sim$110 mm after the lens). For the HASO, the lenslet array should be positioned at this plane; for the IR NF camera, it should be the sensor; and for the IR FF line, it should be the focussing lens.

Figure 8 a) shows the inherent wavefront error due to the full relay imaging line (P-V 0.006λ), b) shows the expected distortions in the image, and c) shows the PSF on axis, with a FWHM of $\sim$34 μm. If a CCD with 9.9 μm pixels (e.g. AVT Manta) is used, the PSF is $\sim$3.4 pixels, meaning that the system will be approaching detector-limited resolution. The demagnification of the full HASO imaging system is 55, so the resolution at the object plane will be of the order of 0.72 mm. In the current design, the NF/FF channel gives near identical results. The telescopes can be easily modified if different output beam diameters are required. Provided that the f/# of the system is kept relatively large, a wide range of beam diameters should be achievable without any degradation in performance.

The need to split the beam into three separate diagnostic channels after the relay telescope for NF, FF, and wavefront, means that only one of the channels will achieve the performance shown above, whilst the other two channels necessarily be imaging through at least one beamsplitter at 45 degree AOI. This introduces aberrations into those channels for the purpose of imaging, and if wedged beamsplitters are used, may introduce some angular dispersion. It is still possible to get acceptable resolution on all three channels, and to combat angular dispersion, although the performance of each channel need to be considered when deciding which diagnostic should be assigned to which channel. In order to reduce aberrations, as mentioned above, an iris can be placed after the final lens of the relay telescope, or separate irises could be used for each channel to allow individual optimisation. The elimination of angular dispersion can be achieved by the use of a second wedge with an equal but opposite wedge angle. This could be in the form of a dedicated compensation plate, or by placing the diagnostic on a channel which naturally incorporates transmission through two beamsplitters.

B-integral

A key consideration in the diagnostic design is the effect of B-integral. On a full power shot, the energy in the leakage beam ($\sim$60 mJ) will be high enough to accumulate B-integral in any transmissive optics: the leakage mirror substrate, the vacuum chamber window, and the wedge [M3] on the diagnostics table. While B-integral in the mirror substrate is unavoidable, there are options to limit the B-integral in the window and the wedge. The B-integral in the mirror substrate depends on the transmission of the HR coating, and the substrate thickness. The transmission of the coating can only be reliably controlled down to $\sim$0.2%. Lower transmission coatings can be made, but the transmission will be unknown until measured after manufacture. It is preferred to have control over the exact transmission, because if the transmission is too low the diagnostic will be insensitive to alignment beams. Also, limiting ourselves to a controllable transmission means a damaged mirror can be replaced without risking the sensitivity of the diagnostics. The optic thickness is limited by manufacturing concerns, with the EPAC mirrors requiring a thickness of at least 35 mm. For a transmission of 0.2%, the expected B-integral in the leakage mirror substrate would be between 0.41 and 0.58 depending on the value taken for non-linear index. The range of values used here is 2.5 $\times$ 10^{-16} and 3.5 $\times$ 10^{-16} cm^2 / W [8, 9], which is acceptable. However, a similar B-integral will be acquired in both the vacuum window and wedge, leading to a total B-integral of $\sim$1.4 for all three optics. In order to mitigate this, the vacuum window will be specified with a partially reflective coating. A 90% reflective coating would reduce the contribution of the window and wedge by a factor of 10, bringing the total B-integral down to 0.67, which would be acceptable for this diagnostic. It should be noted that due to stretching of the pulse in the transmissive media, the B-integral calculated here is an upper estimate.

Main beam pointing stabilisation

Good pointing stability of the EPAC main beam onto target is a critical requirement for reliable delivery of the laser-driven sources in EA1. While the EA1 beamline has been designed to have high mechanical and ther-

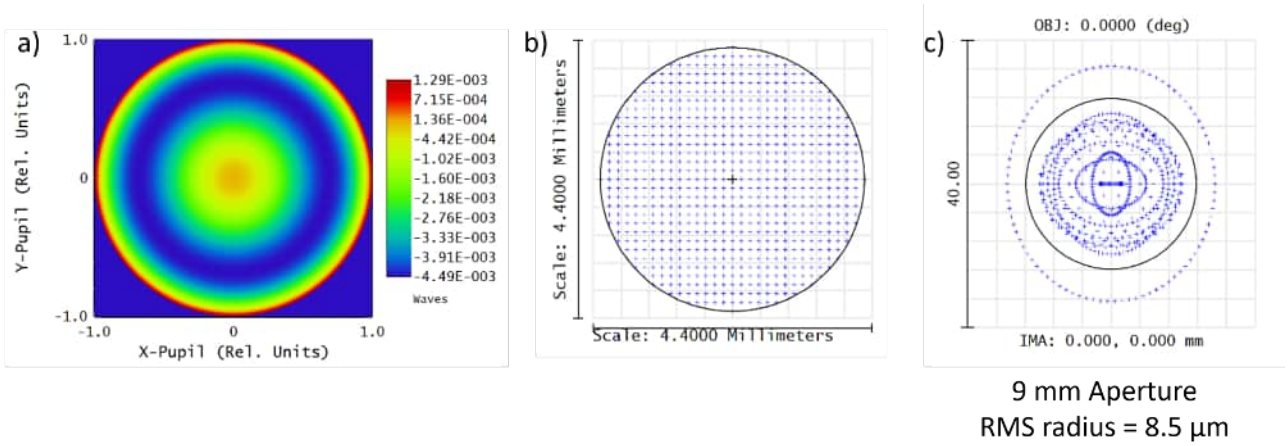

Figure 7: a) Wavefront map at the image plane of the collimation lens; b) beam footprint illustrating the image distortions; c) raytrace of the system assuming an on-axis point-source 50 m from the leakage mirror, the RMS diameter is ∼17 μm.

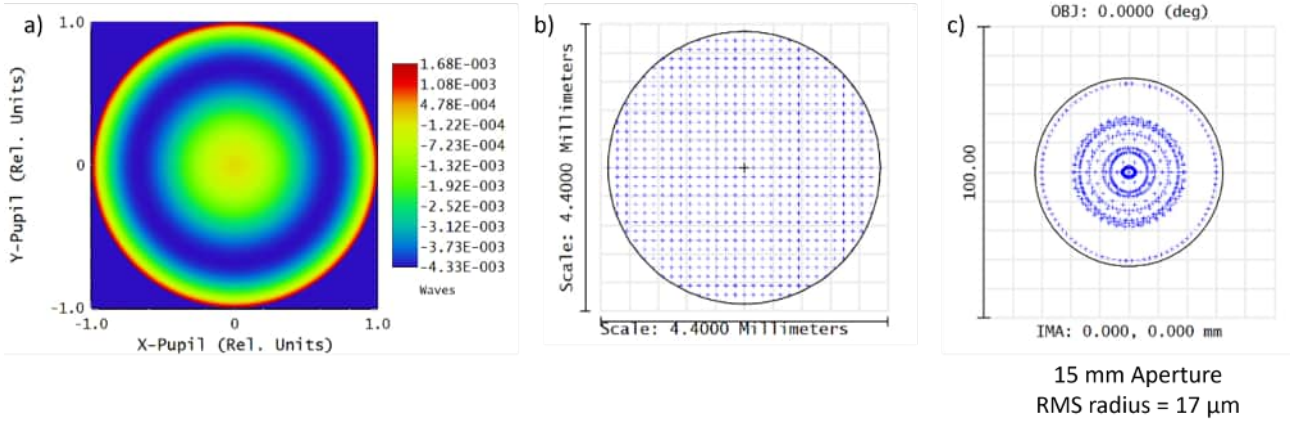

Figure 8: Wavefront map at the image plane of the image relay telescope on the main diagnostic channel; b) beam footprint illustrating the distortions in the image; c) raytrace of the system for an on-axis point 50 m upstream of the leakage mirror, the RMS radius is ∼34 μm, resulting in a resolution of ∼1.12 mm at the object plane.

mal stability – by using granite support blocks and rigid mounting – there will always be some drift and jitter in the laser beam delivered into the area. A scheme has been designed to actively stabilise beam pointing throughout the laser system on fast (jitters) and slow (drifts) timescales. The final section of the beam path into the Experimental Areas has been designed to use an overlapped 405 nm (blue) CW beam that passes through the compressor and the beam transport line[1]. The leakage of this blue beam into the monitoring diagnostic is focused onto a PSD that can provide feedback to a piezoelectric correction mirror in the laser area. (Alternatively the blue beam can be produced and expanded in EA1 and back-propagated to a PSD in the laser). Pointing fluctuations caused within the diagnostic itself should be measureable using the internal EA1 beam and accounted for in the feedback control software. It is hoped that the mechanical stability in EA1 means that whatever pointing performance is achieved at the reference point in the diagnostic will be maintained onto target. If this scheme fails, then a backup option is to use a reference within the target chamber as close as possible to the target position. A method for achieving this has been implemented on the Bella laser to continuously measure on-shot beam stability [2]. This is complicated in our case because the baffles used for differential pumping on the entrance path to the target chamber restrict where a pilot beam can propagate. In addition, because EPAC operates as a user facility, beam configurations and target equipment will frequently change and that makes it difficult to maintain a critical optical set up close to the

[1]Note that the proposal to use a 405 nm laser is dependent on sourcing dichroic beam transport optics with sufficient damage threshold for EPAC. This may be changed to an 800 nm CW pilot beam and chopper wheel system, in which case the diagnostic scheme will be modified accordingly.

interaction point.

The layout we would use in EA1 is shown in Fig. 10, using the reflection of the pilot beam from the rear surface of the final turning mirror to monitor stability. The separation of the beams at focus depends only on their relative angular separation, while in the region before focus, their footprint positions are determined by both the angular separation and the lateral displacement due to the spatially separated points of reflection, and is therefore dependent on the substrate thickness. As the substrate thickness is already driven by two counter-acting concerns – the substrate must be as thin as possible to avoid B-integral, but thick enough for manufacture – the only variable parameters for optimising the design are the magnitude and direction of the wedge. We limit ourselves to only having the wedge along the long axis of the optic to constrain all beam deviation, whether due to refraction or reflection, to the horizontal plane – this is preferred from a practical standpoint. The wedge can then have two orientations. In one orientation, the angular displacement of the pilot beam w.r.t. the main beam will serve to further separate the beams as they travel, while in the other orientation the pilot beam displacement will reduce as the beams travel, up to the point that they cross, after which point separation will begin to increase again. The choice of magnitude and direction of the wedge is driven by a few factors. Firstly, it is preferable for the beams to be as closely overlapped as possible at the AO and the OAP to avoid clipping of the pilot beam by optic apertures. Secondly, the beam must be sufficiently separated from the main beam in the target chamber that a pick-off mirror can be inserted to re-direct the pilot beam before reaching focus. If both beams passed through the same aperture in the baffles, then they would be too close together near focus, preventing a diversion of the pilot beam. This means that the beams need to be sufficiently separated when they reach the first baffle that windows could be inserted into the baffles to transmit the pilot-beam. (Alternatively, the baffle could be made of optical quality glass with a central hole and the pilot beam would pass through the glass.) These considerations have led to our final design using a wedge of 4 arcmins, oriented so that the pilot beam and main beam will cross after a certain travel distance. For the 10 m focal length OAP that will be used for EPAC commissioning, the crossing point will be nearly mid-way between the AO and OAP, ensuring good overlap on both. Moving to shorter or longer focal lengths will move the crossing point towards the AO or OAP respectively, but maintain a reasonable overlap on both. With this design, the beam diameter at the first baffle is 22 mm, and the main beam and pilot beam will be separated by 39 mm, leaving a 17 mm gap between the beams. Baffles made of optical glass will probably be needed to transmit the pilot beam to focus. An additional feature of this scheme is that, given the good overlap of the pilot beam and the main beam at the AO, it would be possible to use the pilot beam not only as a measure of stability, but also as a constant monitor of the AO surface during full power shots. This would be simple to implement after the beam is picked off in the target chamber.

Exit mode diagnostics

For some experiments it is important to characterise the spatial and spectral properties of the laser pulse exiting the plasma. Spectral modifications such as red- and blue-shifting provide information about the plasma, and an exit-mode diagnostic is very useful for monitoring the operation of waveguides. The standard technique for LWFA experiments [3] is to allow the exiting beam to propagate to a size large enough that an uncoated optic can reflect a portion of it without damage. On Gemini we have typically used a wedged window placed $\sim {}^{2}/_{3}$ of the focal length after the exit of the target. A hole drilled in the centre of the optic allows electrons and x-rays to pass uninhibited. Of order 4 – 10 % (depending on polarisation) of the beam is reflected without damage to the surface, while the remainder of the beam passes through to a beam-block. The B-integral accumulated through the substrate is not an issue because the beam is dumped afterwards. Because of the higher repetition rate of EPAC, we will place the first optic almost a full focal length after the target – but it is not yet known if damage to the bulk substrate will build up making this method impractical for long term operation at 10 Hz. An alternative arrangement is to fold the exiting beam using two plasma mirrors to return the beam on a parallel path to the incoming beamline. This has the key advantage of removing the laser directly after the target, protecting downstream components (such as magnets) and leaving the subsequent beampath clear of obstacles. The energy losses from the double plasma mirror help with the issue of fluence through the first exit mode optic. The development of plasma mirrors that can operate at high repetition rate with high quality reflection (using tape drives or liquid sheets) is an ongoing project by CLF and other groups worldwide [4]. We will also consider the option to trigger the plasma mirror to increase its reflectivity and decrease the amount of debris produced [5]. Both of these configurations will use the same optical arrangement to attenuate and collimate the beam exiting the plasma. In the direct exit-mode, the chamber will be located in EA1-A and reflected horizontally to an optical table holding the diagnostics. In the folded exit-mode the chamber is placed close to the adaptive optic chamber with the beam exiting vacuum vertically through a hole in a breadboard supporting the diagnostics above the beamline. Because this will be less stable than the direct exit-mode, it may not be suitable for some guided LWFA experiments.

The in-vacuum optics are shown in Fig. 11. The beam is reflected from two 10" diameter, 40 mm thick fused

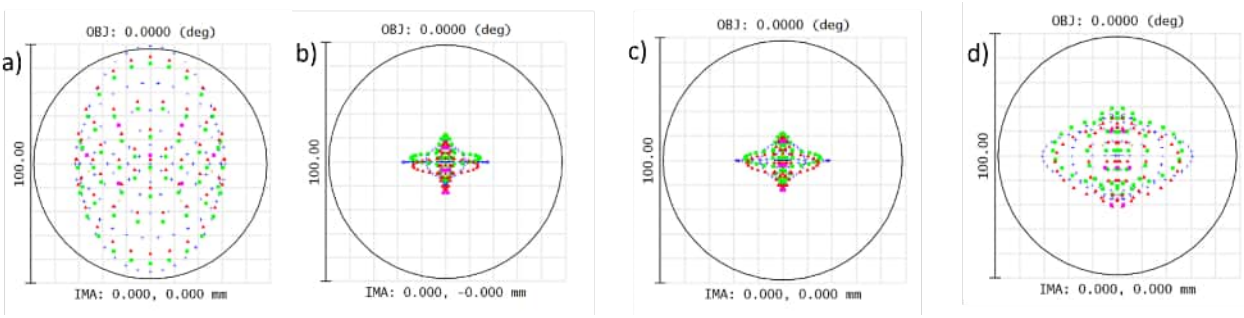

Figure 9: Raytrace spots of point sources at image plane of relay telescope with a) 1 beamsplitter with 30 arcmin wedge b) 2 beamsplitters with 30 arcmin wedges oriented in opposite directions, c) 1 beamsplitter with 30 arcsec wedge (Eksma standard) and d) 2 beamsplitters with 30 arcsec wedges oriented in opposite directions.

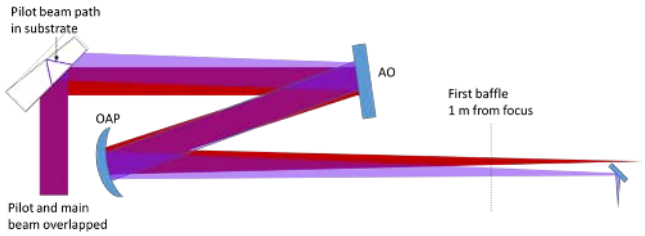

Figure 10: Schematic of proposed scheme for stability beam to include AO and OAP in pilot beampath.

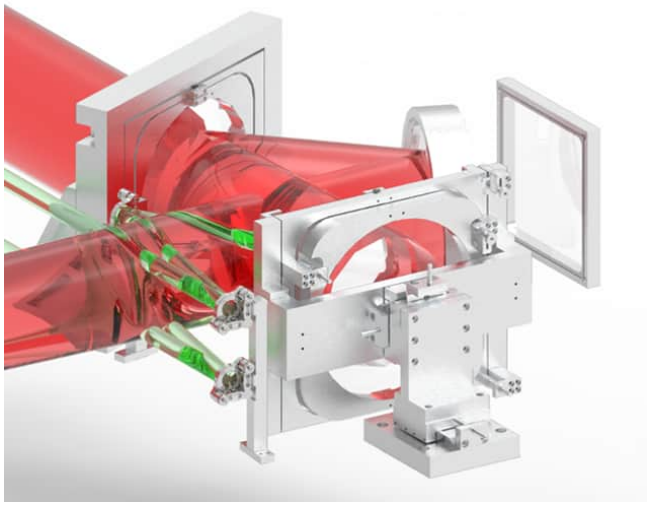

Figure 11: Layout of the in-vacuum optics (two uncoated wedged windows and a spherical mirror) used to attenuate and collimate the beam exiting the plasma.

silica uncoated wedged windows, reducing the energy by a factor of ∼100 (for p-polarisation). It is collimated with a 10" diameter, 8,250 mm focal length (f / 37), silver coated spherical mirror that reflects the beam back through the second wedge to exit the chamber through a vacuum window. The beam diameter for a 10 m focal length beamline will be ∼180 mm, although this might be modified by the plasma. The first optic has a large wedge angle of 2 degrees to help separate the front and rear surface reflections. For the second optic, we use a small wedge angle of 6.4 arcmin because the beam is also transmitted. The angle was chosen to match the wedge in the input beam diagnostic for convenience. Behind the first wedge most of the energy in the beam will be dumped on a screen, calorimeter, or cooled beam dump depending on operational fluence. Before the spherical mirror, two 1" mirrors will divert pick-off beams that can be used for measurements that are affected by transmission through optics. One of these lines will be collimated and exit through a thin (1 mm) window for pulse shape measurements. Pulse compression is expected in the plasma [6] so this line will be equipped with a Swamp Optics Grenouille (8-9 or 8-20 models) for ultrafast pulse characterisation. The second line could be used for long wavelength (> 2 micron) measurements – usually these need to exit vacuum through a specialist window (e.g. ZnSe).

After passing through the vacuum window, the beam enters a diagnostic arrangement (Fig. 12) that is similar to the input beam diagnostics. This uses the same focusing system of passing through a wedge (6.4 arcmin) onto a 6,600 mm silver-coated spherical mirror – again the optic specification is chosen to match the input beam diagnostic for convenience. We have calculated the angular dispersion through the pair of wedges and do not expect this to be a problem. The same optical design for energy control, collimation, and image relaying provides channels for NF, FF, wavefront, and energy measurements. An additional beam is directed to a spatially resolved optical spectrometer because plasma-induced features in the spectrum could be non-uniform. The spectral range of a compact spectrometer (Andor Shamrock 163) using a 600 lines/mm grating is 256 nm with 0.37 nm resolution. This is expected to be suitable for most experiments [7]. Space is available for the Grenouille or a similar compact device. If a larger spectrometer (e.g. for mid-IR measurement) is required, this can be placed on the optical table in the direct-mode or on the

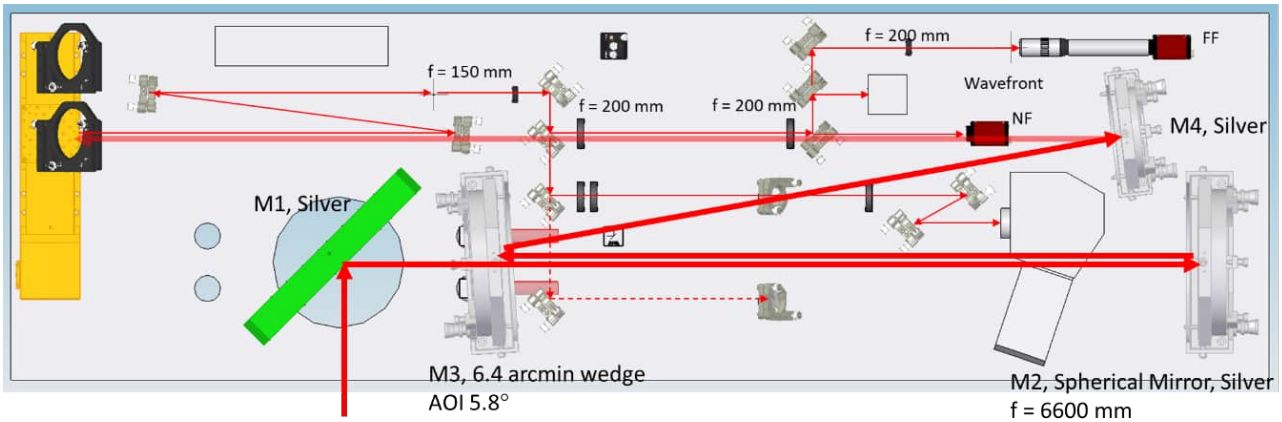

Figure 12: Proposed design for the layout used in the EA1 beamline for monitoring the beam exiting the plasma.

lower level of the support frame for the folded-mode. The lower level could also be used to accommodate alternative pulse duration measurement devices, e.g. FC-Spider, which would be too large to fit on the upper table.

Conclusion

We have presented the optical design for diagnostics that will be used to measure the laser beam properties in the EPAC EA1 beamline. Assisted by Zemax modelling, we have ensured that aberations in the diagnostic channels are minimised so that the diagnostics provide an accurate representation of the beam. Stability is a key issue, and during installation we will need to ensure that fluctuations in pulse properties are true rather than diagnostic artefacts. The diagnostic set-ups have been designed so that they can work both with low-power alignment modes and with the full laser energy. In this way they can be used for daily alignment as well as acting as on-shot references.

References

[1] D. R. Symes *et al.* EPAC Experimental Areas and Targetry Developments. *CLF Ann. Rep.* 2021/22.

[2] F. Isono *et al.* High-power non-perturbative laser delivery diagnostics at the final focus of 100-TW-class laser pulses. *High Power Laser Science and Engineering*, **9**, e25 (2021).

[3] K. Nakamura *et al.* Diagnostics, Control and Performance Parameters for the BELLA High Repetition Rate Petawatt Class Laser. *IEEE Journal of Quantum Electronics*, **53**, pp. 1-21, (2017).

[4] A. Zingale *et al.* Emittance preserving thin film plasma mirrors for GeV scale laser plasma accelerators. *Phys. Rev. Accel. Beams* **24**, 121301 (2021).

[5] G. F. H. Indorf *et al.* Investigation of the ejected mass during high-intensity laser solid interaction for improved plasma mirror generation. *Plasma Phys. Control. Fusion* **64**, 034004 (2022).

[6] J. Schreiber *et al.* Complete Temporal Characterization of Asymmetric Pulse Compression in a Laser Wakefield. *Phys. Rev. Lett.* **105**, 235003 (2010).

[7] A. J. Ross *et al.* Resonant excitation of plasma waves in a plasma channel. *arXiv:2310.05097*, (2023).

[8] S. Santran *et al.* Precise and absolute measurements of the complex third-order optical susceptibility, *JOSA B*, **21**, 2180 (2004).

[9] M. J. Weber, D. Milam, and W. L. Smith, Nonlinear Refractive Index Of Glasses And Crystals, *Opt. Eng.*, **17**, 463 (1978).